

## Multiple Axis Boom Crane Maneuver Generation for Payload Swing Suppression\*

**Michael J. Agostini**

**Gordon G. Parker**

**Erin E. Kruse**

Michigan Technological University:

ME-EM Department

Houghton, MI 49931

(906) 487-1850, (906) 487-2822, agostini@mtu.edu

**Hanspeter Schaub**

**Kenneth Groom**

**Rush D. Robinett**

Sandia National Laboratories:

Albuquerque, NM 87185

(505) 844-0739, (505) 844-6161, kngroom@sandia.gov

### ABSTRACT

This paper considers the generation of open-loop inputs for multiple axis, swing-free movement of crane payloads. A particular crane is considered having a geometry that results in payload dynamic equations that are nonaffine in the crane inputs. Unlike previously considered systems with affine in the input swing dynamic equations, a closed form, symmetric solution is not generally available. Therefore, a basis function optimization process is used to generate the crane input time histories given the initial and desired final configurations. Of particular interest is the effect of the nonideal joint-level servo dynamics. Instead of constraining the crane commands to be within the servo's linear regions, saturation can and should be exploited to achieve short time maneuvers. Using an experimentally verified crane simulation, residual swing is shown to be virtually eliminated when nonideal joint dynamics are considered. When these phenomenon are neglected during the maneuver generation process the final residual swing suffers.

### INTRODUCTION

Cranes are used throughout the transportation and construction industry ranging in application from light-duty, small motion lift-assistance to multiple ton, large motion payload placement seen in construction operations. In general, the payload acts as a spherical pendulum whose attachment point is maneuvered using the crane's degrees-of-freedom. As the operator commands the various axes of the crane to affect rigid body payload translation and rotation, the payload's swing degrees-of-freedom can be excited. An experienced operator can often generate the correct crane inputs such that the payload is swing-free at the end of the maneuver. Training an operator, using a

crane, requires significant resources and potential hazards. In contrast, an operator-in-the-loop simulator could be used as a preliminary training tool to reduce costs and increase safety.

The motivation for this work is the development of a simulation based, crane operator training system. Although a simulation system has the potential for aiding operator training, it should not merely replicate the payload motions caused by the operator. In addition, it should suggest to the user the best operator inputs for performing a specified maneuver. For this application, swing-free maneuver histories do not need to be computed in real-time. Instead, they can either be stored in a database, or generated on-call, but with a computational delay between specifying the maneuver end points and generating the maneuver time history.

Although a crane system is the focus of this work, the dynamic phenomenon is common to a variety of systems. For example, satellites with flexible solar panels and robots positioning flexible payloads exhibit similar motion of their respective oscillatory subsystems. Therefore, the proposed approach may have more general applicability than crane input generation.

The relationship of the payload's swing dynamics, to the rigid body inputs, can vary widely. For example, an overhead gantry crane with constant cable length is affine in the trolley acceleration input [1]. For this system, closed-form, open-loop, symmetric input time histories have been found that result in residual swing-free motion of the payload. Some systems with nonaffine payload dynamics have also been shown to have symmetric residual swing-free input histories for specific maneuvers [2], [3].

The crane considered in the following study is allowed to

\*This work was supported by NSWC Carterock under contract DE-AC04-94AL 85000.

have general, multi-axis maneuvers, and because of its geometry, its payload dynamics are nonaffine in the input even for slow maneuvers. Because of these complexities, closed-form solutions have not been found. Instead, an optimization approach is used to generate minimum residual swing, bang-coast-bang acceleration profiles. A coordinated point-to-point payload repositioning maneuver is used to demonstrate the effectiveness of the approach.

Previous work in optimal crane maneuver generation has relied on perfect actuator dynamics. In practice, this is far from the case. Nonideal actuator dynamics, caused by speed saturation and relatively low bandwidth, lead to distortions in the bang-coast-bang accelerations realized by the crane, and residual oscillation in the payload. Two approaches for circumventing this are investigated. The first is to choose a sufficiently slow maneuver, within the crane's joint bandwidth, and without saturation. The second approach is to exploit the saturation as part of the input resulting in a shorter maneuver time. The importance of considering these limits is illustrated.

For all three examples results are presented using an experimentally verified dynamic simulation of a 1/16th scale boom crane. Residual swing is quantified in terms of its magnitude as a fraction of the maximum swing angle encountered during the maneuver.

## PAYLOAD DYNAMICS

The crane is shown in Figure 1 where the three speed inputs are (1) slew rate,  $\dot{\alpha}$ , (2) luff rate,  $\dot{\beta}$ , and (3) hoist rate,  $\dot{L}_h$  (in this study, the hoist rate is zero). The outputs of interest are the payload's tangential and radial swing angles, (measured relative to the boom)  $\theta_1$  and  $\theta_2$  respectively, as shown in Figure 1. The orientation of the hoist frame  $\{h\}$  results from an  $X$ - $Y$  Euler angle rotation sequence relative to the boom frame  $\{\beta\}$ .

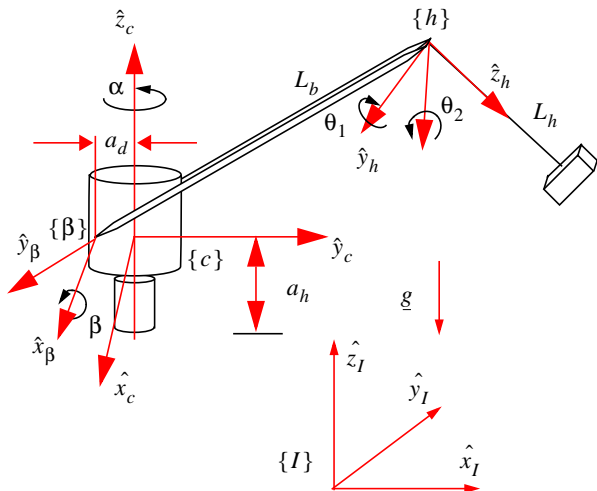


Figure 1: Slew, Luff and Hoist

Ideally the payload should be at rest at the end of any

particular payload repositioning maneuver. Any deviation from the vertical configuration results in swing error in both the radial and tangential direction, as defined in Equation 1.

$$\begin{aligned} e_1 &= \theta_1 \\ e_2 &= \theta_2 + \beta \end{aligned} \quad (1)$$

The payload's dynamic equations of motion are required for the trajectory development and are shown in Equation 2 and 3 after linearizing in swing angles and rates. The inputs are the positions, velocities, and accelerations of the crane degrees of freedom and the crane parameters shown in Table 1.

Table 1: Crane Parameters

$a_d$	0.017 m
$L_b$	2.37 m
$L_h$	1.0 m

$$\begin{aligned} L_h \ddot{\theta}_1 + 2L_h \dot{\alpha} \dot{\theta}_2 + \\ (g + L_b \ddot{\beta} \cos \beta - L_h \dot{\beta}^2 \sin \beta - L_h \dot{\alpha}^2) \theta_1 + \\ L_h \dot{\alpha} \dot{\theta}_2 = L_b (2\dot{\alpha} \dot{\beta} \sin \beta - \dot{\alpha} \cos \beta) \end{aligned} \quad (2)$$

$$\begin{aligned} L_h \ddot{\theta}_2 - 2L_h \dot{\alpha} \dot{\theta}_1 - L_h \dot{\alpha} \theta_1 + \\ (g + L_b \ddot{\beta} \cos \beta - L_h \dot{\beta}^2 \sin \beta - L_h \dot{\alpha}^2) \theta_2 = \\ L_b ([\dot{\alpha}^2 + \dot{\beta}^2] \cos \beta + \dot{\beta} \sin \beta) \end{aligned} \quad (3)$$

## SERVO DYNAMICS

A block diagram of the 1/16th scale crane testbed servo model for slew, luff and hoist is shown in Figure 2 where  $\dot{\theta}_c$  is commanded speed (for any axis),  $V_b$  is a constant to account for motor amplifier bias and slight gravity effects in luff and hoist,  $\dot{\theta}_m$  is the actual drive system speed,  $F_s$  is a nonlinear saturation function,  $F_{dz}$  is a nonlinear dead-zone function,  $V_m$  is the motor voltage,  $K_p$ ,  $K_I$  and  $K_f$  are the servo controller gains, and  $K_m$ ,  $\tau_m$  are the motor/amplifier gain and time constant respectively.

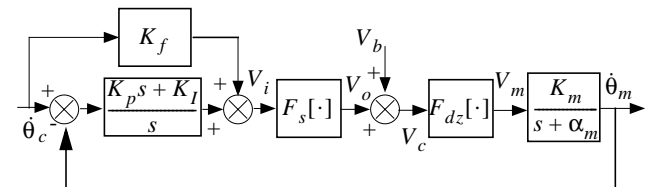


Figure 2: Drive System Servo Model

The time-domain equations for the model, suitable for implementation in a numerical simulation are

$$(K_p + K_f) \dot{\theta}_c - K_p \dot{\theta}_m + K_I (\theta_c - \theta_m) = V_i \quad (4)$$

$$V_o = F_s(V_i) \quad (5)$$

$$V_c = V_o + V_b \quad (6)$$

$$V_m = F_{dz}(V_c) \quad (7)$$

$$\tau_m \ddot{\theta}_m + \dot{\theta}_m = K_m V_m \quad (8)$$

The saturation function,  $F_s$ , is described by

$$V_o = \begin{cases} V_{o, max} & V_i \geq V_{o, max} \\ V_i & V_{o, min} < V_i < V_{o, max} \\ V_{o, min} & V_i \leq V_{o, min} \end{cases} \quad (9)$$

and  $F_{dz}$  is a nonlinear dead-zone function described by

$$V_o = \begin{cases} V_c - V_{dz} & V_c > V_{dz} \\ 0 & -V_{dz} < V_c < V_{dz} \\ V_c + V_{dz} & V_c < -V_{dz} \end{cases} \quad (10)$$

The form of the model is the same for luff, slew, and hoist. The only differences are the parameters  $K_p, K_I, V_b, K_m, \alpha_m$ , which are listed in Table 2.

Table 2: Joint Servo Model Parameters

	Luff	Slew	Hoist
$K_f$ (volt/°/sec)	0.0056	0.0053	0.0050
$K_p$ (volt/°/sec)	0.02	0.05	0.02
$K_I$ (volt/°)	0.025	0.005	0.025
$V_{o, min/max}$ (volt)	-11.3/+11.3	-10/+10	-10/+11
$V_{dz}$ (volt)	0	0.35	0
$V_b$ (volt)	-1.85	-0.33	0.50
$K_m$ (°/sec/(volt))	143	145	177
$\alpha_m$ (sec) <sup>-1</sup>	100	100	100

The model was experimentally verified and accurately predicts unsaturated and saturated servo speed behavior with less than 3% error.

## MANEUVER GENERATION PROCESS

The general approach is to use an optimization code to choose maneuver defining parameters. The optimization code cost function is based on the crane simulation where the inputs to the simulation are the maneuver parameters, selected by the optimization process, and the output is the integral of the root of the squared error ( $e$ ) of the residual payload swing. These elements are discussed in more detail in the remainder of this section.

### Basis Function Design

Bang-coast-bang acceleration basis functions are used for

the luff and slew crane inputs ( $\beta$  and  $\alpha$ ), as shown in Figure 3. The free variables, selected by the optimization process, are the two pulse widths ( $t_{p_1}, t_{p_2}$ ) and the final time of the maneuver,  $t_f$ . Each axis (luff and slew) is allowed to have different values for these quantities, resulting in a total of 6 free optimization parameters.

The maneuver start time for both axes is assumed to be the same (time zero), and the final distance traveled by each axis is specified. This generates two constraint equations for each axis as shown in Table 3.

Table 3: Constraint Equations

Slew	Luff
$t_f = t_{p_1} + t_{p_2} + t_c$	$t_f = t_{p_1} + t_{p_2} + t_c$
$p_\delta = a_p t_p \left( \frac{1}{2} t_{p_1} + \frac{1}{2} t_{p_2} + t_c \right)$	$p_\delta = a_p t_p \left( \frac{1}{2} t_{p_1} + \frac{1}{2} t_{p_2} + t_c \right)$

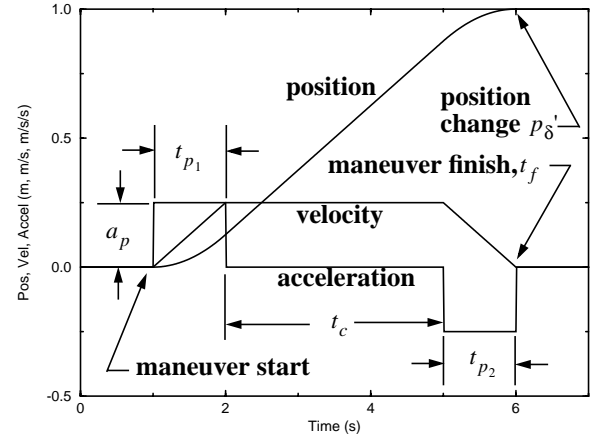


Figure 3: Bang-Coast-Bang Basis Function

### Cost Function

The absolute swing error  $e$ , is used as the metric for determining swing performance.

$$e = \sqrt{e_1^2 + e_2^2} \quad (11)$$

The cost function is the integral of  $e$  from the end of the maneuver,  $t_f$ , to a time four pendulation periods after the end of the maneuver, thus penalizing residual swing information.

$$\Gamma = \int_{t_f}^{t_f + 4(2\pi\sqrt{L_h/g})} e dt \quad (12)$$

Swing during the course of the maneuver is not a factor in the cost, only the residual swing.

A real-time, operator-in-the-loop dynamic simulation called CraneSim was constructed in C. Payload swing is computed using the full nonlinear dynamic equations as

opposed to the linearized version of Equation 1 and 2. It allows general operator inputs and external disturbances (e.g. wind, container lifting transients, etc.). In addition, the crane speed servos (on luff, slew, and hoist) are modelled as described previously. An external numerical constrained optimizing code uses CraneSim for cost function evaluation. This capability allows one to optimize a wide variety of parameters including crane geometric design parameters.

## RESULTS

The intent of this section is to illustrate different methods for compensating for the nonideal joint dynamics, and to explore the feasibility of generating inputs by ignoring the joint effects.

The first approach is to generate maneuvers that avoid nonideal the actuator behavior. Specifically, to ensure that the joint speeds do not saturate. Of course, this results in a slower maneuver as compared to allowing saturation. Crane inputs are generated using ideal actuator dynamics, then applied to the simulation where the nonlinear joints are modeled. This is compared to generating a comparably slow maneuver using the full nonlinear joints when evaluating the cost function.

The second approach is to allow the joint speeds to be unconstrained. Again, the maneuver is first generated without joint effects in the cost function model. This solution is then evaluated using the full nonlinear simulation. Crane inputs are then generated using a cost function simulation that contains the nonlinear joint effects.

### Test Case Description

The test case coordinated maneuver consists of lowering the boom from 65 to 35 degrees and simultaneously slewing from 0 to 40 degrees. A typical example is shown in Figure 4. To quantify the amount of residual swing suppression, the fraction of the magnitude of the residual swing is compared to the largest swing angle occurring during the maneuver. This is used so that the results can be scaled to larger hoist line lengths.

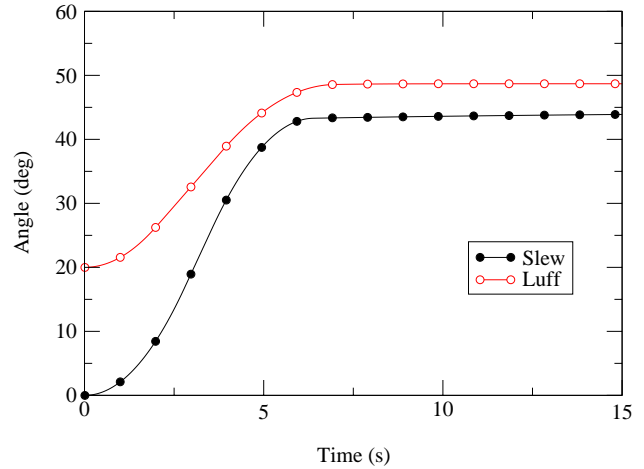


Figure 4: Typical Multi-Axis Maneuver

### Method 1: Saturation-Free Maneuvers

The optimization process was performed twice: (1) assuming perfect joint dynamics, and (2) using the joint dynamic model. However, the joints were not allowed to saturate. The parameters defining the maneuver are shown in Table 4. In both cases the total maneuver time is nearly the same (5.88 seconds for the optimization without actuator dynamics and 5.78 seconds for optimization with joint dynamics). This indicates, as expected, that ignoring the joint dynamics is valid, as long as the system is not saturating.

Table 4: Optimal Parameters for Coordinated Maneuver

Parameter	Optimized without Actuator Dynamics		Optimized with Actuator Dynamics	
	Slew	Luff	Slew	Luff
$t_{p_1}$ (sec)	3.19	2.84	3.46	2.39
$t_{p_2}$ (sec)	1.93	1.46	1.99	1.69
$t_f$ (sec)	5.88	5.31	5.78	5.36

The joint accelerations and swing angles for both cases are shown in Figure 5 and Figure 6. The residual swing error fraction is similar for both as shown in Table 6. This indicates, as expected, that ignoring the joint dynamics is appropriate when the maneuver is not allowed to cause speed saturation.

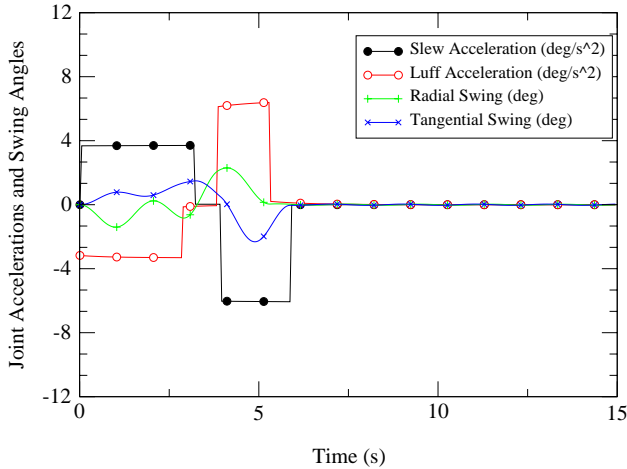


Figure 5: Joint accelerations and swing angles where the maneuver parameters were found assuming no actuator dynamics, but tested in a simulation where the joint dynamics were modeled. Joint rates were not allowed to saturate.

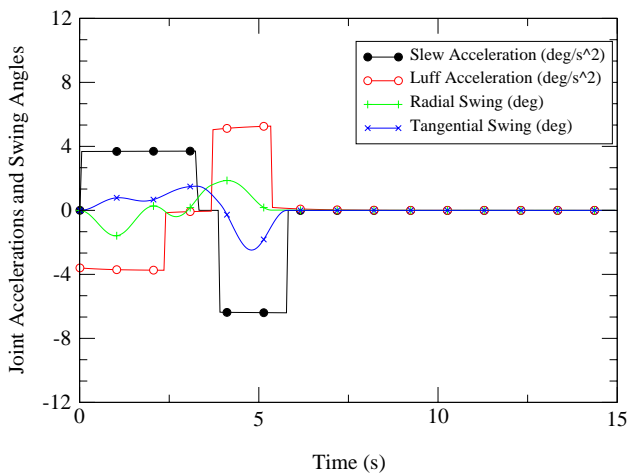


Figure 6: Joint accelerations and swing angles where the maneuver parameters were found using a simulation that included the actuator dynamics. Joint rates were not allowed to saturate.

Table 5: Residual swing error fraction for method #1.

	Residual swing error fraction	
	Tangential	Radial
Optimized without Actuator Dynamics	1.56	1.74
Optimized with Actuator Dynamics	0.24	0.64

### Method 2: Saturation Maneuvers

Again, the optimization process was performed twice: (1) assuming perfect joint dynamics, and (2) using the joint dynamic model. However, the joints rates were allowed to take on any value. This resulted in theoretically shorter

maneuvers than the previous example. The parameters defining the maneuver are shown in Table 5. In both cases the total maneuver time is nearly the same (4.56 seconds for the optimization without actuator dynamics and 4.66 seconds for optimization with joint dynamics).

Table 6: Optimal Parameters for Coordinated Maneuver

Parameter	Optimized without Actuator Dynamics		Optimized with Actuator Dynamics	
	Slew	Luff	Slew	Luff
$t_{p_1}$ (sec)	1.67	1.84	1.73	1.59
$t_{p_2}$ (sec)	1.92	1.68	2.58	1.28
$t_f$ (sec)	4.56	4.04	4.66	3.47

The joint accelerations and swing angles for both cases are shown in Figure 7 and Figure 8. The residual swing error fraction is significantly larger for the case where saturation was ignored during the maneuver generation (Table 7).

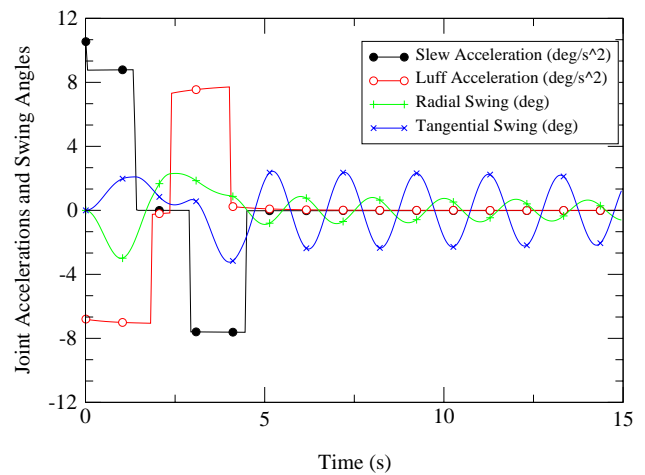


Figure 7: Joint accelerations and swing angles where the maneuver parameters were found assuming no actuator dynamics, but tested in a simulation where the joint dynamics were modeled. Joint rates were allowed to take on any value.

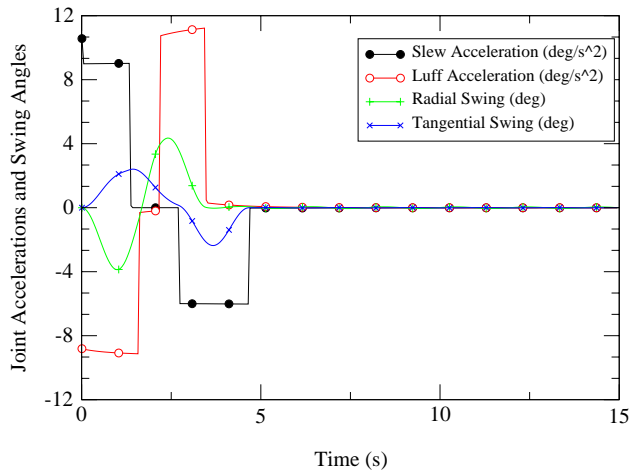


Figure 8: Joint accelerations and swing angles where the maneuver parameters were found using a simulation that included the actuator dynamics. Joint rates were allowed to take on any value.

Table 7: Residual swing error fraction for method #2.

	Residual swing error fraction	
	Tangential	Radial
Optimized without Actuator Dynamics	75.2	35.7
Optimized with Actuator Dynamics	1.25	0.96

## CONCLUSION

A method for generating residual swing-free, open-loop inputs for a crane system was demonstrated. This approach was used, instead of an analytical solution, as the system was nonaffine in the inputs, and no assumptions were enforced regarding the symmetry of the maneuver.

Since the joint characteristics were known, dominated by speed saturation and finite bandwidth, their effect in the optimization process was investigated. Specifically, two approaches were employed. The first was to simply ensure that the commands avoided the speed saturation of the crane joints. As expected, this resulted in similar residual swing performance regardless of the whether or not the actuator dynamics were explicitly used during the optimization. The resulting total maneuver times were approximately 5.8 seconds.

The second approach was to allow large speed commands. This resulted in maneuvers of approximately 4.6 seconds (26% speed increase as compared to the first approach). However, when employing this method it is essential that the true joint dynamics be considered. When they were ignored during the optimization process, the residual swing error fraction was large.

In summary, joint speed saturation can be exploited when

developing swing-free commands. However, the actuator model must be known with sufficient accuracy.

## REFERENCES

- [1] Strip, D. R., 1989, "Swing-Free Transport of Suspended Objects: A General Treatment," *IEEE Transactions on Robotics and Automation*, Vol. 5, No. 2, April 1989, p. 234-236.
- [2] Petterson, B. J. and Robinett, R. D., 1991, "Model-Based Damping of Coupled Horizontal and Vertical Oscillations in a Flexible Rod," *Journal of Intelligent and Robotic Systems*, Vol. 4, 1991, p. 285-299.
- [3] Parker, G. G., Robinett, R. D., Driessen, B. J., and Dohrmann, C. R., "Operator-in-the-loop Control of Rotary Cranes," Proceedings of the 1996 International Society for Optical Engineering Symposium on the Smart Structures and Materials; Industrial and Commercial Applications of Smart Structures Technologies, Sand Diego, CA, Feb. 27-29, Vol. 2721, pp. 364-372.